

LYMPHOID NEOPLASIA

IAP dependency of T-cell prolymphocytic leukemia identified by high-throughput drug screening

Marcel Fabian Pohly,^{1,2} Kerstin Putzker,³ Sebastian Scheinost,⁴ Lena Ben Taarit,⁴ Tatjana Walther,⁴ Sandra Kummer,¹ Tobias Wertheimer,⁵ Minqi Lin,⁵ Thi Huong Lan Do,¹ Kristina Handler,² Jan Michler,² Jarno Kivioja,¹ Karsten Bach,² Samanta Kisele,⁶ James Kim,⁶ Sascha Dietrich,^{7,9} Beat Bornhauser,⁶ Wendy Wei-Lynn Wong,¹⁰ Burkhard Becher,⁵ Andreas Moor,² Joe Lewis,^{3,11} Xenia Ficht,² Junyan Lu,^{7,8,12} Wolfgang Huber,^{8,12} and Thorsten Zenz¹

¹Department of Medical Oncology and Hematology, University Hospital and University of Zurich, Zurich, Switzerland; ²Department of Biosystems Science and Engineering, ETH Zurich, Basel, Switzerland; ³Chemical Biology Core Facility, European Molecular Biology Laboratory, Heidelberg, Germany; ⁴Molecular Therapy in Hematology and Oncology, Department of Translational Oncology, National Center for Tumor Diseases and German Cancer Research Centre, Heidelberg, Germany; ⁵Department of Inflammation Research, Institute of Experimental Immunology, and ⁶Department of Pediatric Oncology, University Children's Hospital, University of Zurich, Zurich, Switzerland; ⁷Medical Faculty Heidelberg, Heidelberg University, Heidelberg, Germany; ⁸Genome Biology Unit, European Molecular Biology Laboratory, Heidelberg, Germany; ⁹Department of Hematology, Oncology and Clinical Immunology, University Hospital of Düsseldorf, Düsseldorf, Germany; ¹⁰Department of Molecular Life Sciences, University of Zurich, Zurich, Switzerland; ¹¹Anavo Therapeutics, Heidelberg, Germany; and ¹²Molecular Medicine Partnership Unit, Heidelberg, Germany

KEY POINTS

- T-PLL and other T-cell lymphomas are sensitive to drugs that target autophagy, nuclear export, and IAPs.
- IAP inhibition induces an upregulation of the NF-κB pathway in T-PLL, with subsequent cell death being primarily necroptotic.

T-cell prolymphocytic leukemia (T-PLL) is an aggressive lymphoid malignancy with limited treatment options. To discover new treatment targets for T-PLL, we performed high-throughput drug sensitivity screening on 30 primary patient samples ex vivo. After screening >2800 unique compounds, we found T-PLL to be more resistant to most drug classes, including chemotherapeutics, than other blood cancers. Furthermore, we discovered previously unreported vulnerabilities of T-PLL. T-PLL cells exhibited a particular sensitivity to drugs targeting autophagy (thapsigargin and bafilomycin A1), nuclear export (selinexor), and inhibitor of apoptosis proteins (IAPs; birinapant), sensitivities that were also shared by other T-cell malignancies. Through bulk and single-cell RNA sequencing, we found these compounds to activate the Toll-like receptor (bafilomycin A1), p53 (selinexor), and tumor necrosis factor α (TNF- α)/NF-κB signaling pathways (birinapant) in T-PLL cells. Focusing on birinapant for its potential in drug repurposing, we uncovered that IAP inhibitor-induced cell death was primarily necroptotic and dependent on TNF- α . Through spectral flow cytometry, we confirmed the absence of cleaved caspase-3 in IAP inhibitor-treated T-PLL cells and show that IAP inhibition reduces the proliferation of T-PLL cells stimulated ex vivo, while showing only a limited effect on nonmalignant T-cells. In summary, our study maps the drug sensitivity of T-PLL across a broad range of targets and identifies new therapeutic approaches for T-PLL by targeting IAPs, exportin 1, and autophagy, highlighting potential candidates for drug repurposing and novel treatment strategies.

Introduction

T-cell prolymphocytic leukemia (T-PLL) is an aggressive T-cell lymphoma characterized by the proliferation of mature, postthymic T-lymphocytes.¹ Its clinical course is usually rapid, with progressive lymphocytosis, splenomegaly, and lymphadenopathy.¹ T-PLL response to conventional chemotherapy is poor, and remissions induced with the monoclonal anti-CD52 antibody alemtuzumab are rarely maintained.¹ With a median overall survival of <20 months,^{1,2} there is an urgent need to identify new treatment strategies. High-throughput ex vivo drug screening enables the systematic assessment of drug sensitivities in blood cancers. Previous studies identified T-PLL

sensitivity to the B-cell lymphoma 2 (Bcl-2) homology 3 (BH3) mimetic venetoclax, p53 activators, as well as inhibition of histone deacetylase (HDAC) or the Janus kinase (JAK)-signal transducer and activator of transcription (STAT) pathway.³⁻⁷ Early clinical data, however, suggest that these compounds are insufficient to provide long-term control of the disease, illustrating the need for additional treatment options.^{6,8,9} We have previously reported on the ex vivo drug sensitivity of several blood cancers, including T-PLL.⁵ Here, we present a resource of 5 ex vivo drug screening data sets, along with a reanalysis of the previous data. In total we capture T-PLL drug response to >2800 unique compounds. We combine these data with combinatorial drug perturbations, bulk RNA sequencing

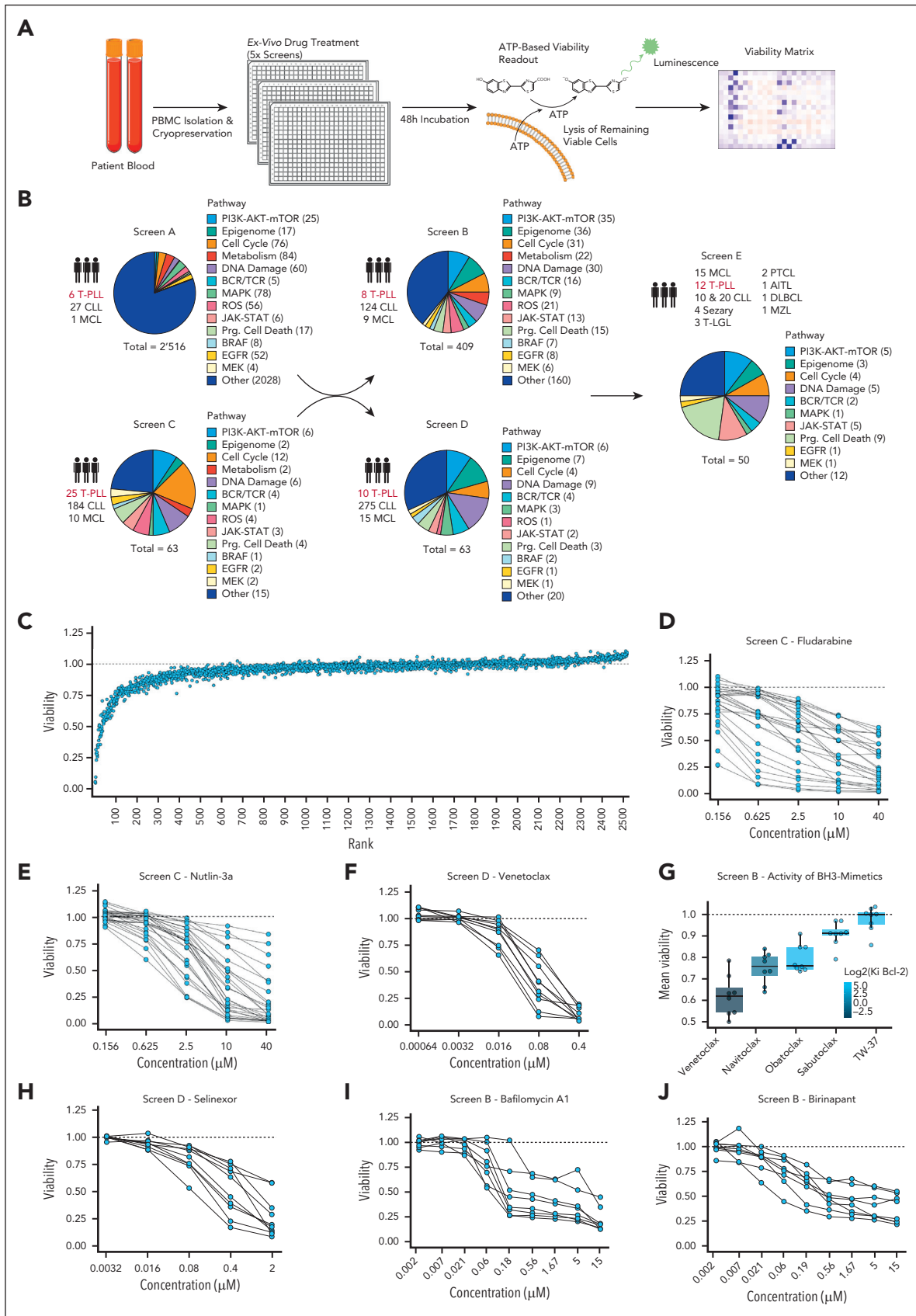


Figure 1. Overview and drug response landscape of T-PLL. (A) Schematic overview of the ex vivo drug screens. PBMCs with tumor cells were isolated from patient blood and cultured with drugs for 48 hours ex vivo, before cell viability was measured based on adenosine triphosphate-dependent luminescence. (B) Overview of the patient samples and drug libraries used for screens A through E. (C) Cell viability of 6 patient-derived primary T-PLL samples in screen A. Viabilities are relative to a DMSO negative control after

(RNA-seq) and single-cell RNA-seq (scRNA-seq), as well as spectral flow cytometry, to study previously undescribed T-PLL pathway dependencies, including a particular sensitivity to inhibitor of apoptosis protein (IAP) inhibition.

Methods

Ex vivo drug screens

Drug screens were conducted using viably frozen peripheral blood mononuclear cells (PBMCs) following previously described protocols.⁵ Details on the screens, the bulk RNA-seq, scRNA-seq, and spectral flow cytometry experiments can be found in the supplemental Methods, and supplemental Tables 2 and 4, available on the *Blood* website. Targeted sequencing of *TP53* and western blots were performed using previously published approaches and are detailed in the supplemental Methods.^{10,11}

Data analysis

The preprocessing and analysis of drug screen data, including quality filtering, normalization, incubation effect correction, drug-drug correlation, and the testing for synergistic or antagonistic drug combinations followed previously published approaches and are detailed in the supplemental Methods.^{5,12}

Study approval

The study was approved by the ethics committees in Heidelberg, Germany (University of Heidelberg; S-206/2011; S-356/2013) and Zurich, Switzerland (2019-01744).

Results

Drug sensitivity of primary T-PLL cells

To capture T-PLL drug sensitivities, we measured the drug response of 9 primary blood cancers in 5 drug screens ex vivo (referred to as screens A, B, C, D, and E, respectively). This included the previously published screen C, which we reanalyzed with a focus on T-PLL.⁵

For each screen, PBMCs were isolated from the blood and cultured with drugs for 48 hours, before cell viability was assessed by measuring adenosine triphosphate (Figure 1A). Screen A used a library of 2516 drugs, including therapeutics, kinase inhibitors, and clinically used and investigational compounds, and was performed on 34 patient samples ($n_{T\text{-}PLL} = 6$; Figure 1B). Screen B contained primarily small-molecule inhibitors ($n = 409$) with multiple compounds per drug class at a wider concentration range in 141 patient samples ($n_{T\text{-}PLL} = 8$). Screens C and D were performed with a subselection of 63 compounds each, representing key drug classes, in a greater number of patient samples ($n_{\text{Patients Total}} = 219$ [screen C], 300 [screen D]; $n_{\text{Patients T-PLL}} = 25$ [screen C], 10 [screen D]).

Finally, 50 drugs were chosen for the testing in a wider set of T-PLL ($n = 12$) and T-cell malignancies ($n = 10$), referred to as screen E (Figure 1B).

A full list of the compound libraries and the key screen characteristics is provided in Table 1, and supplemental Tables 1 and 2.

We began our analysis by ranking drugs based on their effect on viability. Of 2516 compounds in screen A, only a small fraction ($n = 253$; 10%) decreased the mean viability (v) of T-PLL patient samples by >10% and only 99 (3.9%) by >25% (Figure 1C). This limited response to drugs was observed across screens (supplemental Figure 1A-F).

Most tyrosine kinase inhibitors demonstrated little activity, even when used at high concentrations (>10 μM). This included the JAK1/2 inhibitor ruxolitinib and the phosphoinositide 3-kinase inhibitor duvelisib, 2 drug candidates for the treatment of T-cell lymphoma (mean viability [$v_{\text{Screen B}}$] = 0.95, 0.95; supplemental Figure 2A-B).^{4,18,19} Chemotherapeutics were among the most toxic drugs. This included drugs used to treat T-PLL such as the antimetabolites cytarabine ($v_{\text{Screen B}} = 0.78$) and fludarabine ($v_{\text{Screen C}} = 0.55$; Figure 1D; supplemental Figure 1F).^{1,20} Previous studies reported T-PLL sensitivity to p53 activation, BH3-mimetics, and HDAC inhibition.^{3,5,6} In line with this, the p53 activator nutlin-3a was highly active across screens ($v_{\text{Screen C}} = 0.63$); however, some patient samples appeared to be resistant (Figure 1E). Because *TP53* mutation is a common mechanism of nutlin-3a resistance, we performed targeted sequencing of the *TP53* gene, but did not detect any mutations (Table 1).^{5,21} The Bcl-2 inhibitor venetoclax induced a more pronounced decrease in viability than other BH3 mimetics (navitoclax, obatoclax, sabutoclax, and TW-37), which possess a broader range of targets (Bcl-xL, Bcl-w), but lower binding affinity for Bcl-2 (screen B; adjusted P value <.001; Figure 1F-G).¹³⁻¹⁷ This is in line with reports that describe T-PLL to primarily rely on the anti-apoptotic signal of Bcl-2.^{4,6} We confirmed the sensitivity of T-PLL to HDAC inhibitors (ie, panobinostat, $v_{\text{Screen B}} = 0.65$), while also uncovering a susceptibility to other classes of epigenetic modifiers; specifically, histone demethylase (JIB04), histone methyltransferase (UNC0638), and BET inhibitors (OTX015, JQ1; $v_{\text{Screen B}} = 0.68, 0.8, 0.85$, and 0.86, respectively; supplemental Figure 1E-F).³ Notably, we observed a high degree of correlation when comparing the drug response between screens for overlapping patient samples and compounds ($R^2 = 0.59-0.81$; supplemental Figure 2C).

We also uncovered previously undescribed pathway dependencies. T-PLL was especially vulnerable to nuclear export (selinexor and verdinexor), autophagy (thapsigargin and baflomycin A1), and IAP (birinapant and GDC-0152) inhibition

Figure 1 (continued) treatment with 2516 drugs averaged over all concentrations ($n = 2-6$). Drugs were ranked based on their median decrease in cell viability (across all patient samples and concentrations) from most lethal (left) to mostly neutral (right). (D) Dose response curves showing the viability of patient-derived T-PLL samples ($n = 25$, each line represents a patient) to fludarabine relative to a DMSO negative control. Corresponding dose response for T-PLL samples to nutlin-3a ($n = 25$) (E) and venetoclax ($n = 10$) (F). (G) Varying activity of different BH3 mimetics in 9 patient-derived T-PLL samples. Color hues show the \log_2 -transformed inhibitory constant (K_i) of each compound for the antiapoptotic protein Bcl-2.¹³⁻¹⁷ A small K_i indicates high binding affinity between an inhibitory ligand and its receptor. Dose response curves showing the viability of patient-derived T-PLL samples to selinexor ($n = 10$) (H), baflomycin A1 ($n = 8$) (I), and birinapant ($n = 8$) (J). ATP, adenosine triphosphate;AITL, angioimmunoblastic T-cell lymphoma; AKT, alpha serine/threonine kinase; BCR, B-cell receptor; BRAF, B-Raf proto-oncogene, serine/threonine kinase; DLBCL, diffuse large B-cell lymphoma; EGFR, epidermal growth factor receptor; MAPK, mitogen-activated protein kinase; MEK, mitogen-activated extracellular signal-regulated kinase; mTOR, mammalian target of rapamycin; MZL, marginal zone lymphoma; PI3K, phosphoinositide 3-kinase; Prg., programmed; PTCL, peripheral T-cell lymphoma; ROS, reactive oxygen species; TCR, T-cell receptor.

Table 1. Patient sample characteristics

Patient ID	Sex	Age at diagnosis, y	Sample ID	White blood cell count ($\times 10^9/L$)	Lymphocytes, %	Treatment naïve	Immunophenotype (CD4/CD8)	Cytogenetics	TP53 status	Screens used
H358	M	72	13PB0031 13PB0162	65 84	92 97	No No	CD4 ⁺		wt	Screen A, screen C, screen E Screen D, screen B
H371	M	61	12PB0258 12PB0332 12PB0510	114 137 113	92 92 100	Yes Yes No	CD4 ⁺	46,XY,del(11q22)	wt	Screen E Screen A, screen B, screen C Screen D
H382	M	68	13PB0135			Yes		del(11)(q22.3),t(14;14)	wt	Screen C
H383	F	67	13PB0136			Yes		inv(14)	wt	Screen C
H384	F	78	13PB0137			Yes		del(11)(q22.3),inv(14)	wt	Screen C
H394	M	83	13PB0344			Yes		inv(14)	wt	Screen C
H395	F	75	13PB0345			Yes		del(11)(q22.3),inv(14)	wt	Screen C
H396	F	63	13PB0346			Yes		inv(14)	wt	Screen C
H397	F	42	13PB0347			Yes		del(6)(q21),del(11)(q22.3)	wt	Screen C
H398	F	52	13PB0348			No		inv(14),t(14;14)	wt	Screen C
H399	F	65	13PB0349			Yes		t(X;14)		Screen C
H400	F	74	13PB0350			No		del(11)(q22.3),inv(14)	wt	Screen C
H401	F	70	13PB0352	414	94	Yes	CD4 ⁺ , CD8 ⁺	43-44,X,-X,der(6)t(X;6)(?q;p25), i(8)(q10),del(11)(q13), der(12)t(12;18)(p12;q1??), -13,der(14)t(14;14)(q11;q32), ider(14)t(14;14)(q11;q32), -18,t(21;22)(q21;q2??) [cp8]/46,XX[2]	wt	Screen C
H402	M	83	13PB0356	43	81	Yes	CD4 ⁺	46,XY[4]	wt	Screen C
H403	M	45	13PB0326 13PB0335 13PB0391 13PB0567 13PB0623	87 99 101 161 167	90 91 91 96 95	Yes Yes Yes Yes Yes	CD8 ⁺	46, XY, der(2)t(2;22)(p11)(q11) t(2;8), inv(14)(q11q32), del20(q11q13), der(22)t(2;22) WES	wt	Screen B Screen E Screen A Screen C Screen D
H405	M	72	13PB0404			Yes		add(8)(q24),inv(14)	wt	Screen A, screen C
H406	M	72	13PB0405			No			wt	Screen A, screen C
H408	M	76	13PB0421			Yes		inv(14)	wt	Screen A, screen C

F, female; M, male.

Table 1 (continued)

Patient ID	Sex	Age at diagnosis, y	Sample ID	White blood cell count ($\times 10^9/L$)	Lymphocytes, %	Treatment naïve	Immunophenotype (CD4/CD8)	Cytogenetics	TP53 status	Screens used
H417	M	62	13PB0547			Yes		inv(14),t(14;14)	wt	Screen D, screen C, screen E
H424	F	57	14PB0058 14PB0094	106 126	88 86	Yes No	CD4 ⁺ , CD8 ⁺	43-46,XX,del(2)(p23)[4],-3[5],add(6)(q13)[4],-8 ×2[10],-12[8],der(13;15)(q10;q10)[4],-14 ×2[12],-15[7],-16[6],-18[12],-19[5],-20 ×2[12],-21[6],+8-12mar,inc[cp12]/46,XX[13]	wt	Screen B, screen C Screen D, screen E
H426	F	49	14PB0110 14PB0113			Yes Yes		del(11)(q22.3),t(14;14)	wt	Screen C Screen C
H427	M	85	14PB0111					del(11)(q22.3),t(14;14)	wt	Screen C
H428	M		14PB0112					del(11)(q22.3),del(17)(p13)	wt	Screen C
H431	M	65	14PB0152 14PB0282	55 88	75	Yes Yes	CD4 ⁺		wt	Screen C Screen D, screen B, screen E
H279	M	56	14PB0323 14PB0329	97 48	86	Yes Yes	CD4 ⁺	46,XY	wt	Screen D, screen C, screen E Screen B
H453	M	67	15PB0242	6	81		CD8 ⁺	46,XY [28]	wt	Screen B
H490	M	90	17PB0227	73	87	Yes		46,XY,del(1)(q14q22), inv(14)(q11q32)[1]/46,XY,sl, add(10)(q27s),add(13)(p11), add(16)(p1?2),add(21)(p11)(cp7)/ 46-47,sd1,der(6)ins(6;?)(p11;?)add(6)(p2? 5),+mar(cp6)/47,sd2, +add(8)(p1?2)cp4/46,XY[1]		Screen D
H492	M	65	17PB0229	55	77	Yes	CD4 ⁺	45-46,XY,add(7)(q3?2),i(8)(q10),+i(8)(q10), -9,-11,add(12)(p1?1),?add(13) (p1?1),inv(14)(q11q3?2),-16,-20,+marx3 [cp4]/46,XY[16]		Screen D
H498	F	75	19PB0007	119	93	Yes	CD4 ⁺	inv(14)(q11;q32)		Screen E
H507	M	77	21PB0017	52	74	Yes	CD4 ⁺	44-45,XY,der(1)t(1;17)(p36.1;q21), add(4)(p16),del(6)(q13),del(8) (p21),ins(11;?)(q13;?),der(11) ins(11;?)(q13;?)t(11;12)(p12;q13), -15,-16,-17,-18,der(21) (q11.2;p11.1),add(22)(p11.2),+r, +2~5mar(cp7)/46,XY[3]		Screen E
H519	F	73	23PB0445	29	66	Yes	CD8 ⁺			Screen E
H521	F	62	23PB0453	35	82	No	CD4 ⁺ , CD8 ⁺			Screen E
H524	M	85	23PB0502	149	73	Yes	CD4 ⁺			Screen E

F, female; M, male.

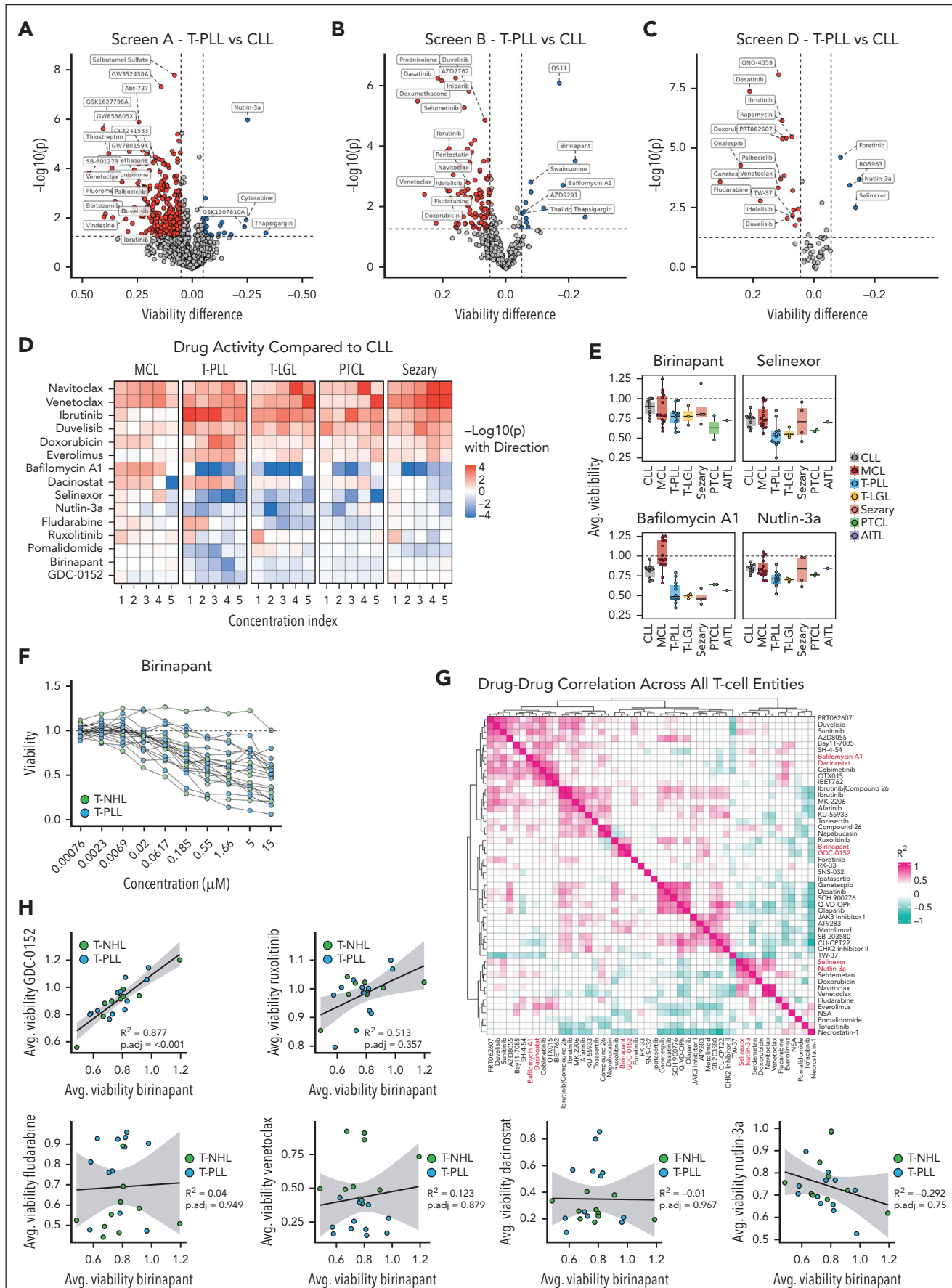


Figure 2.

($v_{\text{screen B}} = 0.74, 0.7, 0.76, 0.75, 0.72$, and 0.83 , respectively; [Figure 1H-J](#); supplemental Figures 1F and 2D).

Identification of T-PLL-specific drug response

We asked which of the drug effects were particularly pronounced in T-PLL by comparing the drug response of T-PLL with that of primary chronic lymphocytic leukemia and mantle cell lymphoma (MCL) samples (2-sided t test; false discovery rate [FDR] of $<10\%$; and mean viability difference = Δ). We found T-PLL to be significantly more resistant to most drug classes, including the clinically used¹ chemotherapeutic fludarabine ($\Delta_{\text{screen D}} = 0.18$; adjusted P value = $.006$), as well as the BH3 mimetics venetoclax ($\Delta_{\text{screen B}} = 0.18$; adjusted P value = $.03$) and navitoclax ($\Delta_{\text{screen B}} = 0.17$; adjusted P value = $.014$; [Figure 2A-C](#); supplemental Figure 3A-D). Only a small set of compounds demonstrated a higher activity in T-PLL: the p53 activator nutlin-3a ($\Delta_{\text{screen A}} = -0.34$; adjusted P value = 3×10^{-5}), thalidomide ($\Delta_{\text{screen B}} = -0.052$; adjusted P value = $.078$), the autophagy inhibitors thapsigargin ($\Delta_{\text{screen C}} = -0.38$; adjusted P value = 3.41×10^{-7}) and baflomycin A1 ($\Delta_{\text{screen B}} = -0.18$; adjusted P value = $.02$), the IAP inhibitor birinapant ($\Delta_{\text{screen B}} = -0.22$; adjusted P value = $.007$), as well as the nuclear export inhibitor selinexor ($\Delta_{\text{screen D}} = -0.13$; adjusted P value = $.01$; [Figure 2A-C](#); supplemental Figure 3A-D). To explore whether these sensitivities are shared by other T-cell malignancies, we performed a validation screen (screen E) using a selection of compounds with T-PLL-specific activity, as well as a diverse range of 50 selective inhibitors and therapeutics in 27 and 22 samples from patients with B-cell and T-cell lymphoma, respectively ([Figure 1B](#)). T-cell lymphoma samples ($n = 10$) demonstrated a response pattern similar to T-PLL ([Figure 2D-E](#)). This suggests that key sensitivities are shared across T-cell malignancies.

Drug-drug correlation suggests distinct mode of action of drug candidates

Based on their pronounced effect on viability and their T-PLL- and T-cell lymphoma-specific activity, we selected birinapant, selinexor, and baflomycin A1 for further exploration. We observed interpatient heterogeneity in the viability effects of these compounds ([Figure 2E-F](#)). To test whether this heterogeneity was simply indicative of overall drug sensitivity, we clustered drugs based on the similarity of their response in T-PLL and T-cell lymphoma samples ([Figure 2G-H](#); supplemental Methods). We found distinct groups of compounds with similar pathway dependencies ([Figure 2G](#)). For instance, birinapant showed significant correlation with GDC-0152, a second, less potent IAP

inhibitor ($R^2 = 0.88$; adjusted P value = 4.1×10^{-6} ; [Figure 2G-H](#)).²² No correlation was observed between birinapant and therapeutics (fludarabine), p53 activators (nutlin-3a and serdemetan), HDAC inhibitors (dacinostat), and BH3 mimetics (venetoclax and navitoclax; [Figure 2G-H](#)). Selinexor demonstrated significant correlation with nutlin-3a, serdemetan, venetoclax, and navitoclax ($R^2 = 0.85, 0.64, 0.56$, and 0.69 ; adjusted P value = $2.6 \times 10^{-5}, .022, .061$, and $.009$, respectively; [Figure 2G](#); supplemental Figure 3E-F). Baflomycin A1, meanwhile, showed high correlation with the HDAC inhibitor dacinostat ($R^2 = 0.73$; adjusted P value = $.005$; [Figure 2G](#)). Combined, these findings indicate similarity in the mode of action of selinexor and p53 activators and BH3 mimetics, as well as baflomycin A1 and HDAC inhibitors. IAP inhibitors, however, appear to act in T-PLL and T-cell lymphoma via a unique mode of action.

Bulk RNA-seq reveals distinct transcriptional responses to drug candidates in T-PLL

To further characterize the drug response to birinapant, selinexor, and baflomycin A1, we treated 9 samples from patients with T-PLL and 1 sample from a patient with T-large granular lymphocytic leukemia (T-LGL) with these compounds as well as 8 specific pathway inhibitors (nutlin-3a, pomalidomide, venetoclax, ruxolitinib, ibrutinib, everolimus, dacinostat, and motolimod, or dimethyl sulfoxide [DMSO]) for 24 hours and performed bulk RNA-seq ([Figure 3A](#); supplemental Figure 3G). To uncover drug effects, we assessed differential gene expression by comparing each condition to the DMSO control (FDR < 10%, $|\log_2 \text{fold change}| > 0.25$; [Figure 3B-C](#); supplemental Figure 4A). The overall number of significantly differentially expressed genes (DEGs) varied greatly between treatments with dacinostat and pomalidomide displaying the highest number of DEGs ($n = 7884, 6569$), whereas other treatments such as nutlin-3a or birinapant showed more restricted expression changes ($n = 682, 203$; [Figure 3B-C](#); supplemental Figure 4A). This was also reflected in the number of significantly upregulated or downregulated pathways as identified by DEG network and gene set enrichment analysis (FDR < 10%; [Figure 3D-E](#); supplemental Figure 4A-F). As expected, treatment with nutlin-3a resulted in a strong upregulation of p53 target genes (BAX, and MDM2, and CDKN1A; [Figure 3E-F](#)). Notably, selinexor showed an overlap with nutlin-3a in terms of DEGs as well as an upregulation of DNA-damage response gene sets ([Figure 3G](#); supplemental Figure 4C-D). This included an upregulation of the TP53 gene itself ($\log_2 \text{FC} = 0.99$; adjusted P value = 6.89×10^{-19}), demonstrating that selinexor acts through the TP53 pathway in T-PLL ([Figure 3G](#)). Treatment with the autophagy inhibitor baflomycin

Figure 2. T-PLL-specific drug response. (A) Differential drug sensitivity of T-PLL ($n = 6$) compared with chronic lymphocytic leukemia (CLL; $n = 27$) samples in screen A. The x-axis shows the average difference in viability; negative values indicate higher sensitivity in T-PLL than in CLL. The y-axis shows the $-\log_{10} P$ value. For each drug, the average across all concentrations was tested. Top associations are labeled, if the difference in viability was $>.05$ and the P value $<.05$, as well as representatives of their drug class. Corresponding plots for screen B (8 T-PLL and 124 CLL samples) (B) and screen D (10 T-PLL and 275 CLL samples) (C). (D) Heat map showing the difference in drug response of MCL ($n = 15$), T-PLL ($n = 12$), T-LGL ($n = 3$), PTCL ($n = 2$), and Sézary lymphoma ($n = 4$) samples compared with that of CLL ($n = 10$) samples in screen E (supplemental Methods). Drug response between diagnosis groups was compared via a t test (null hypothesis: no difference), and 2-sided P values were computed. Hues of the color scale indicate raw P values (red: less, blue: more sensitive than CLL). Values are shown for the 5 highest concentrations (1, highest; 5, lowest). (E) Box plots showing the mean viability (averaged over all concentrations) for CLL ($n = 10$), MCL ($n = 15$), T-PLL ($n = 12$), T-LGL ($n = 3$), PTCL ($n = 2$), Sézary ($n = 4$), and 1 AITL sample after treatment with birinapant, selinexor, baflomycin A1, and nutlin-3a. Each dot is a patient, observations outside the plotting range are censored and shown as triangles. (F) Dose response curve, showing the viability of T-PLL ($n = 12$) and other T-cell lymphoma ($n = 10$) samples after treatment with birinapant across 10 concentrations, normalized to a DMSO negative control. Each line indicates 1 patient. (G) Drug-drug correlation matrix for each pair of drugs used in screen E. The Pearson correlation coefficient (R^2) was computed from the viabilities of the 12 T-PLL and 10 T-cell lymphoma samples after drug treatment (averaged over all concentrations). The rows and columns were arranged based on hierarchical clustering. Key correlation pairs are indicated by color. (H) Correlation plots show the viability (averaged over all concentrations) after birinapant treatment and GDC-0152, ruxolitinib, fludarabine, venetoclax, dacinostat, and nutlin-3a in 12 T-PLL and 10 T-cell lymphoma samples. A trendline is indicated; 95% confidence intervals are shown as shaded gray areas. Avg., average; AITL, angioimmunoblastic T-cell lymphoma; NHL, non-Hodgkin lymphoma; p.adj., adjusted P value; PTCL, peripheral T-cell lymphoma.

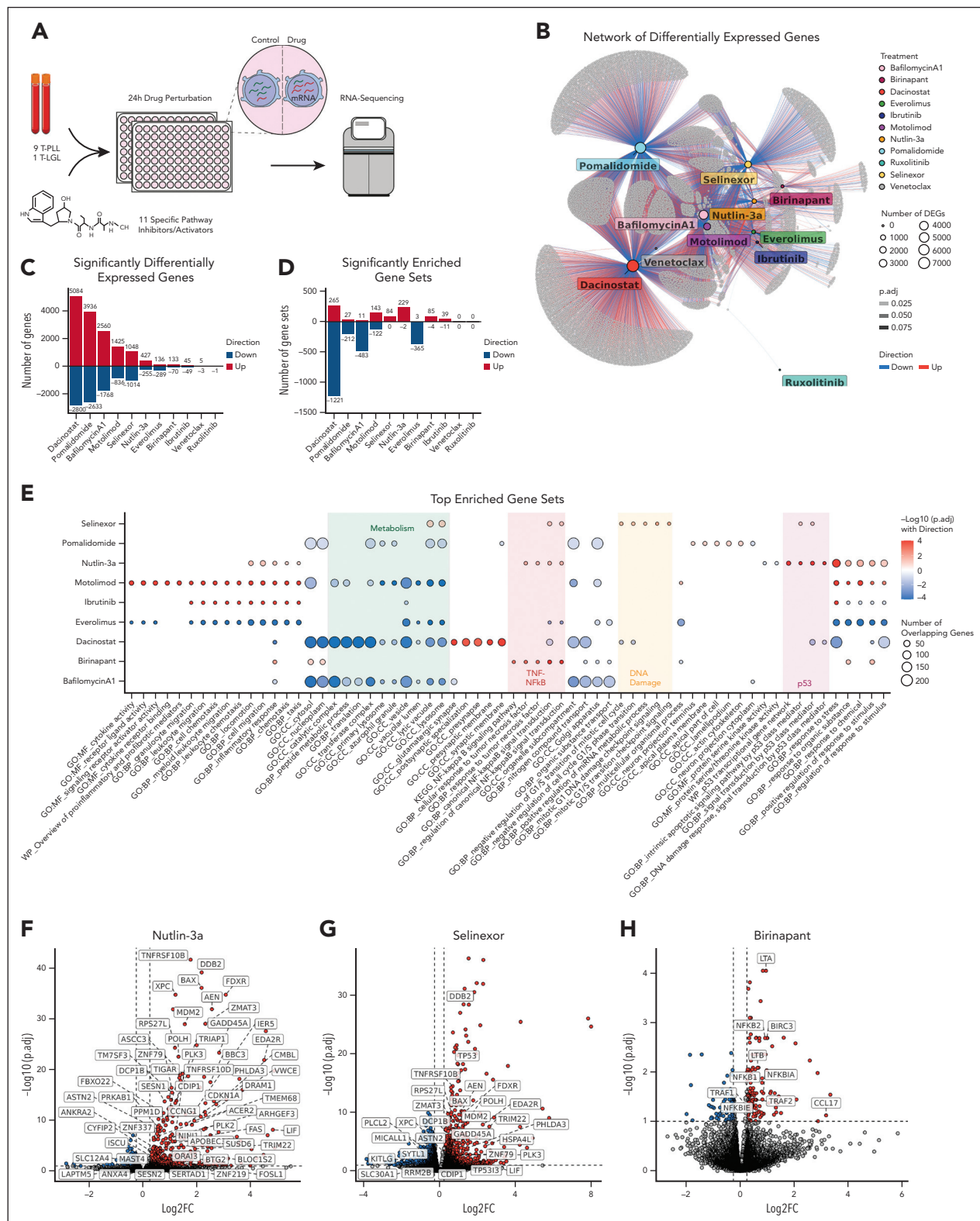


Figure 3. Bulk RNA-seq reveals the landscape of drug effects in ex vivo-treated T-PLL. (A) Schematic overview of the bulk RNA-seq experiment. T-PLL ($n = 9$) and T-LGL ($n = 1$) samples were treated either with birinapant (200 nM), nutlin-3a (2500 nM), motolimod (200 nM), selinexor (200 nM), everolimus (200 nM), ruxolitinib (200 nM), ibrutinib (100 nM), baflomycin A1 (50 nM), pomalidomide (50 nM), dacinostat (5 nM), venetoclax (5 nM), or DMSO for 24 hours followed by RNA extraction, library preparation, and sequencing. (B) Directed network of significantly DEGs (FDR < 10%, $|\log_2\text{FC}| > 0.25$) showing the upregulated and downregulated genes in T-PLL ($n = 9$) and T-LGL ($n = 1$) samples after drug treatment relative to DMSO. In this network, each grey node (dot) corresponds to a DEG, with edges (lines) indicating the treatment(s) (colored nodes) that significantly affected the expression (upregulation = red, downregulation = blue). DEGs that are affected by the same treatments (upregulated or downregulated) are grouped together. Edge thickness indicates the adjusted P value. (C) Bar plot showing the number of significantly DEGs (FDR < 10%, $|\log_2\text{FC}| > 0.25$) after drug treatment relative to DMSO. Upregulated genes are shown as red, downregulated genes as blue. (D) Corresponding bar plot showing the number of upregulated and downregulated

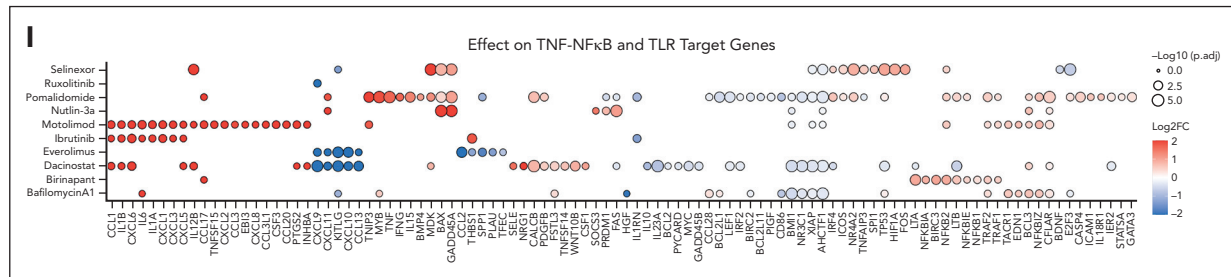


Figure 3 (continued) gene sets. (E) Dot plot showing the top 5 upregulated and downregulated gene sets per treatment (FDR < 10%, ≥10 overlapping genes). Dot size indicates the number of overlapping genes between the DEGs and the gene set. Coloring indicates the $-\log_{10}$ adjusted P value with direction (upregulation = red, downregulation = blue). Dots are arranged by hierarchical clustering. Gene sets belonging to key pathways are highlighted. (F-G) Volcano plots showing the upregulated and downregulated genes after nutlin-3a (F) and selinexor (G) treatment relative to DMSO. DEGs that are known to be upregulated upon p53 pathway activation and the *TP53* gene are labeled.²³ (H) Volcano plot showing the upregulated and downregulated genes after birinapant treatment relative to DMSO. DEGs that are part of the TNF- α and NF- κ B pathways are labeled.²⁴⁻²⁷ (I) Dot plot showing expression changes of DEGs that belong to the TNF- α , TLR, and NF- κ B pathways.²⁴⁻²⁷ Coloring indicates the $-\log_{10}$ adjusted P value with direction (upregulation = red, downregulation = blue). Dots are arranged by hierarchical clustering. p.adj., adjusted P value.

A1 had a strong transcriptional effect on T-PLL cells as judged by the number of DEGs ($n = 4328$). We observed a considerable overlap with the DEGs induced by the Toll-like receptor 8 (TLR8) agonist motolimod (Figure 3B; supplemental Figure 4A,G). Notably, this included an upregulation of several tumor necrosis factor α (TNF- α)/NF- κ B signaling pathway members (*TRAF2*, *BCL3*, and *NFKBIZ*) as well as the proinflammatory cytokine interleukin 6 (*IL6*), which suggests that vacuolar-type adenosine triphosphatase inhibition not only prevents lysosomal acidification in T-PLL but also activates TLR signaling as has been demonstrated for human monocytes (Figure 3I).²⁸

Birinapant inhibits cIAP-1 and cIAP-2, 2 IAP family members that promote apoptosis resistance and cell survival by blocking prodeath signals through the TNF receptor 1, Fas receptor (CD95), and TLR signaling pathways.²⁹⁻³² Birinapant treatment led to a marked upregulation of the TNF- α /NF- κ B signaling pathway (*NFKBIA*, *NFKB1*, *NFKB2*, *TRAF1*, *TRAF2*, and *BIRC3*; Figure 3H-I). Notably, the effect was distinct from that of the TLR8 agonist motolimod, because birinapant treatment only had a limited effect on the expression of TLR-associated proinflammatory cytokines (*IL1A*, *IL1B*, *IL6*, *CXCL1*, *CXCL2*, and *CXCL3*; Figure 3I; supplemental Figure 4H). This is in line with reports, which observed improved tolerability of birinapant over other IAP inhibitors because of birinapant's limited effect on XIAP, a key regulator of inflammasome activation.^{33,34}

Combined, these findings suggest distinct pathway dependencies of birinapant and selinexor on the TNF- α /NF- κ B and p53 pathways, whereas a broader transcriptional effect was observed for baflomycin A1.

Birinapant treatment uniformly affects T-PLL cell transcriptomes

We were intrigued by the potent effects of birinapant on T-PLL and T-cell lymphoma viability as well as the highly specific transcriptional effect. Given birinapant's manageable safety profile in a phase 2 clinical trial,³⁵ it represented a promising treatment candidate, which led us to investigate it further. To capture the effect of birinapant on healthy and malignant cell subsets we treated patient-derived samples (3 T-PLL, 3 MCL, 2 hairy cell leukemia [HCL], and 1 T-LGL) with birinapant and 4 specific pathway inhibitors (nutlin-3a, ibrutinib, everolimus, and

selumetinib, or DMSO) for 48 hours, followed by scRNA-seq (Figure 4A). After quality control, we captured 49 664 cells. For 32 301 (65.0%) cells we additionally retrieved the B- or T-cell receptor sequences. Visualization by uniform manifold approximation and projection embedding revealed a strong separation of T-PLL, HCL, and MCL cells (monoclonal B- and T-cell receptor) from healthy B- and T-cells (polyclonal B- and T-cell receptor; Figure 4B-E; supplemental Figure 5A-F). To assess the transcriptional effect of drug perturbations on nonmalignant T-cells, we randomly sampled an equal number of cells per cell type and treatment, comparing each condition with the DMSO control (FDR < 10%, $|log_2FC| > 0.25$). Comparing the DEGs between cell types (HCL, MCL, T-PLL, and healthy T-cells) demonstrated that the effects of birinapant, ibrutinib, and everolimus were mainly restricted to the malignant cells, whereas nutlin-3a affected both malignant and healthy cell subsets (Figure 4F-J). As a control, we included the BRAF inhibitor selumetinib, which has a strong effect especially on HCL, given the dependency of these cells on a *BRAFV600E* mutation (Figure 4F).³⁶ We found that all lymphoma types and patient samples responded similarly to birinapant, with an upregulation of the TNF- α /NF- κ B pathway, suggesting a conserved transcriptional response to IAP inhibition across lymphoma types (Figure 4K). We observed that this transcriptional response was homogenous across different clusters of malignant cells and did not identify a primary unresponsive subset of T-PLL cells (Figure 4L; supplemental Figure 5G-I). This homogenous pattern of TNF- α /NF- κ B pathway activation contrasts the heterogeneous effects we previously observed for birinapant on cell viability, prompting us to further investigate the mechanisms of cell death in birinapant-treated T-PLL cells.

IAP inhibitors induce necroptosis in T-PLL

The pharmacological or genetic depletion of IAPs has been shown to induce cell death in cancer cells through apoptosis or a form of organized necrosis, termed necroptosis.^{31,37} This process has been linked to the formation of distinct multiprotein signaling complexes, consisting amongst others of FADD, FLIP_S, FLIP_L, caspase-8, RIPK1, RIPK3, and MLKL (Figure 5A).^{31,38,39} To test whether the interpatient heterogeneity in birinapant response may be explained by differential abundances in these proteins, we measured the expression of key apoptotic and necroptotic proteins in samples from patients

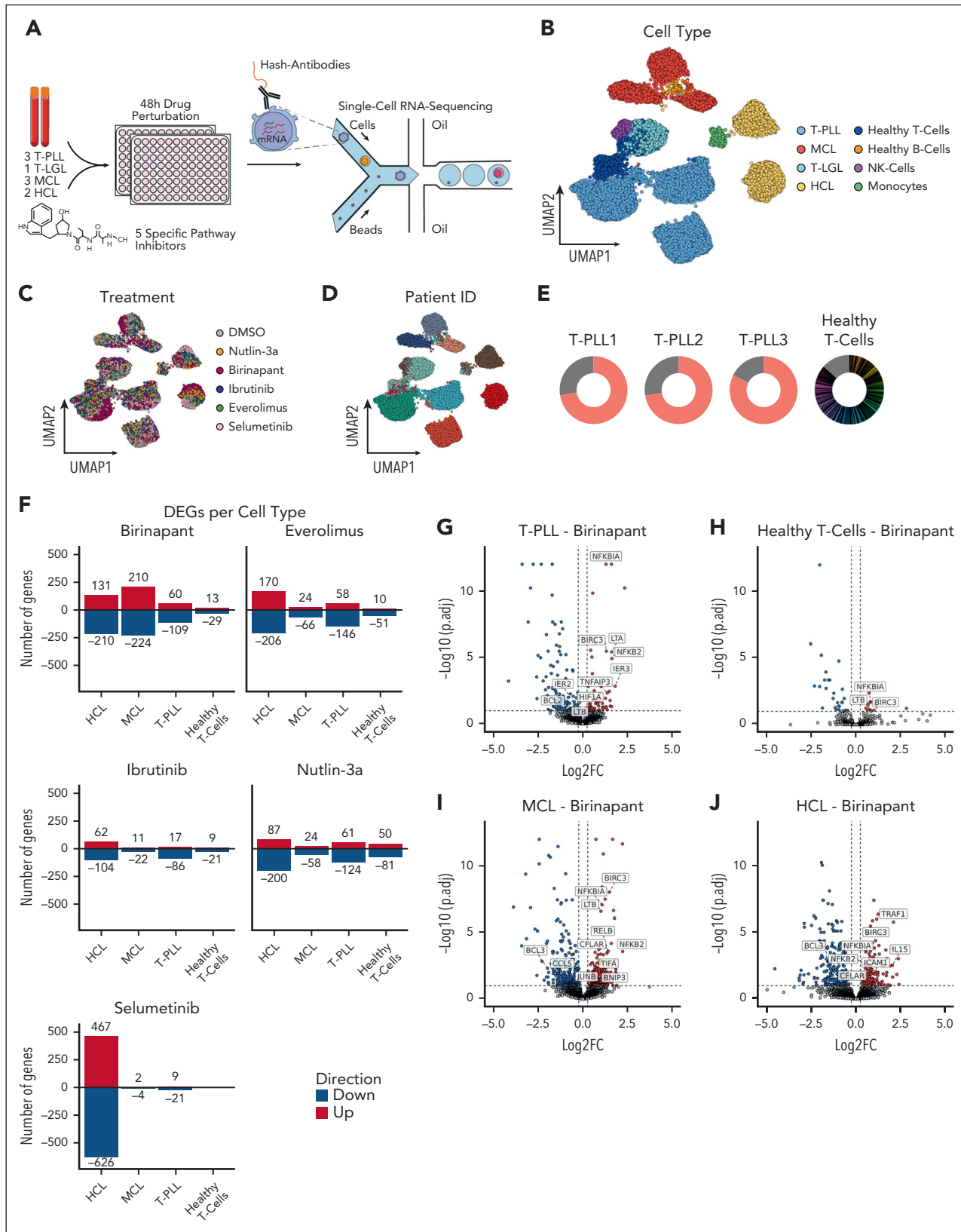


Figure 4. scRNA-seq reveals a uniform transcriptional response across malignant cells. (A) Schematic overview of the scRNA-seq experiment. T-PLL (n = 3), T-LGL (n = 1), MCL (n = 3), and HCL (n = 2) samples were treated either with birinapant (200 nM), nutlin-3a (2500 nM), everolimus (200 nM), ibrutinib (100 nM), selumetinib (625 nM), or DMSO for 48 hours, followed by scRNA-seq. (B) Uniform manifold approximation and projection (UMAP) representation of scRNA-seq data. Cell types are indicated by color. Corresponding UMAP representation colored by treatment (C) and patient ID (D). (E) Donut plots showing the clonal composition based on T-cell receptor sequences of each T-PLL cluster and for healthy T-cells. Cells without available T-cell receptor sequence are shown in gray. Each clone is represented by a different color, the proportion of the

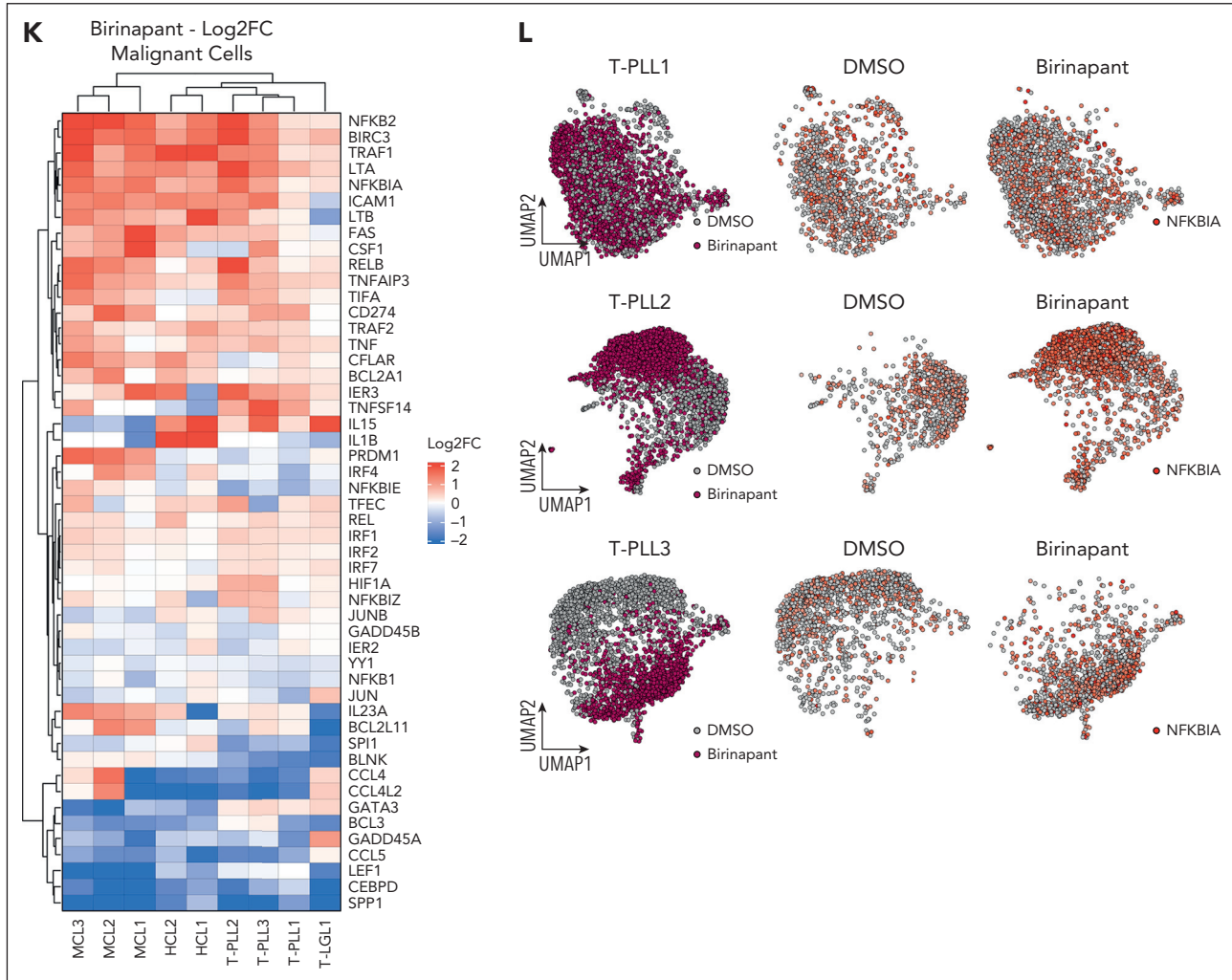


Figure 4 (continued) donut area shaded indicates the size of the clone relative to all cells of the cluster. (F) Bar plots showing the number of significantly DEGs (FDR < 10%, $|\log_2\text{FC}| > 0.25$) relative to DMSO per cell type. An equal number of cells was randomly sampled for each combination of cell type and treatment. Upregulated genes are shown as red, downregulated genes as blue. Volcano plot showing the upregulated and downregulated genes of birinapant-treated T-PLL (G), healthy T cells (H), MCL (I), and HCL cells (J). An equal number of cells was randomly sampled for each combination of cell type and treatment. DEGs that are part of the TNF- α and NF- κ B pathways are labeled.²⁴⁻²⁷ (K) Heat map showing expression changes of DEGs that belong to the TNF- α and NF- κ B pathways,²⁴⁻²⁷ induced by ex vivo drug treatment with birinapant in the malignant cells of each patient sample compared with the matched DMSO negative control. Colors indicate the $\log_2\text{FC}$. (L) UMAP representation showing the malignant cells of patients with T-PLL; T-PLL1 (H371), T-PLL2 (H431), and T-PLL3 (H279); treated with birinapant or DMSO. Colors indicate the treatment (left) as well as the log-normalized expression of NFKBIA (right). ID, identity; h, hour; NFKBIA, NF- κ B inhibitor alpha; p.adj., adjusted P value.

with T-PLL ($n = 8$; Figure 5B; supplemental Figure 6A). We observed variable expression of cIAP1, cIAP2, cFLIP_L, RIPK1, RIPK3, and FADD across T-PLL samples (Figure 5B; supplemental Figure 6A). Notably, we found a trend for association between birinapant response and cIAP2 (BIRC3) and cFLIP_L (CFLAR) expression, which was reflected both on the protein and gene expression levels (protein: $R^2 = -0.41, -0.54$; RNA: $R^2 = -0.65, -0.62$; Figure 5C; supplemental Figure 6B-E). To explore the mode of birinapant-induced cell death in T-PLL, we performed a combinatorial drug screen with specific inhibitors of the apoptosis and necroptosis cascades. For this, we measured the viability of patient-derived samples (11 T-PLL and 1 T-LGL) in response to birinapant at 5 concentrations (0.016–10 μM) as single compound and in combination with the caspase inhibitor, quinoline-val-asp-difluorophenoxy-methylketone (Q-VD-OPh); the RIPK1 inhibitor, necrostatin-1; the RIPK3 inhibitor, GSK-872; and the MLKL oligomerization

inhibitor necrosulfonamide (NSA; Figure 5A). Drug combination synergy and antagonism (cell death blockage) were analyzed using a Bliss independence model (supplemental Figure 6F; supplemental Methods). Necrostatin-1, GSK-872, and NSA but not Q-VD-OPh prevented birinapant-induced cell death in T-PLL (mean combination index [CI] = 1.7, 1.18, 1.37; adjusted P value = .001, .021, .006; Figure 5D-H; supplemental Figure 7A-C). In contrast, Q-VD-OPh addition seemed to further sensitize individual T-PLL samples to IAP inhibitor-induced cell death (CI = 0.94; adjusted P value = .116; Figure 5G-H; supplemental Figure 7D). These findings indicate that IAP inhibitors lead to RIPK1-dependent and necroptotic cell death in T-PLL.^{31,37} Because of the similar transcriptional response of the different lymphoma entities to birinapant treatment in our scRNA-seq data, we asked whether there were differences in the mode of cell death between lymphoma types. For this, we repeated the experiment in a larger set of 49

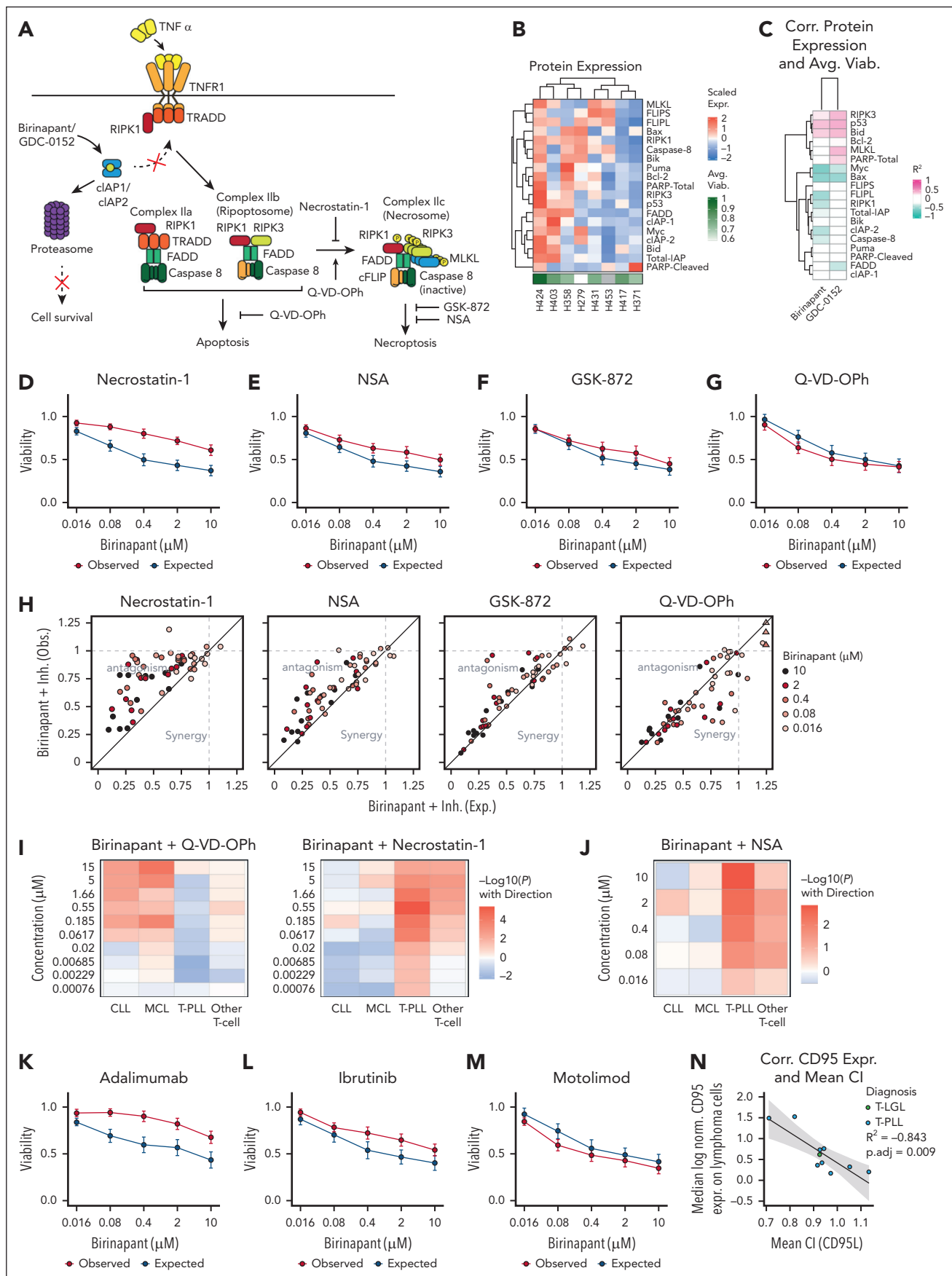


Figure 5.

lymphoma samples ($n_{T\text{-PLL}} = 12$), testing birinapant at 10 concentrations (0.00076–15 μM) alone and in combination with Q-VD-OPh and necrostatin-1. In both T-PLL and T-cell lymphoma, birinapant-induced cell death was decreased upon the addition of necrostatin-1 (CI = 1.35, 1.18; adjusted P value = 3×10^{-4} , 0.058) but not Q-VD-OPh (CI = 0.89, 1.06; adjusted P value = .08, .694; **Figure 5I**). In contrast, caspase inhibition prevented birinapant-induced cell death in MCL and chronic lymphocytic leukemia (CI = 1.21, 1.13; adjusted P value = .041, .016), whereas necrostatin-1 had little effect (CI = 0.99, 0.98; adjusted P value = .288, .076; **Figure 5I**; supplemental Figure 8A). Similar results were obtained when using GDC-0152 instead of birinapant and NSA instead of necrostatin-1 (**Figure 5J**; supplemental Figures 7E and 8B–C). Combined, these findings suggest that IAP inhibitors lead to RIPK1-dependent cell death by necroptosis in T-PLL and other T-cell lymphomas but induce RIPK1-independent apoptosis in B-cell entities.

Birinapant-induced cell death is TNF- α dependent

The antiapoptotic function of IAP proteins involves blocking of prodeath signals through TNF receptor 1, Fas receptor (CD95), and TLRs.^{29–32} Furthermore, autocrine production of TNF- α is required for cell death upon IAP inhibition in many *in vitro* models.^{40,41} To test the relevance of these pathways for IAP inhibitor-induced cell death in T-cell lymphoma, we cultured samples from patients with T-PLL and T-LGL with birinapant at 5 concentrations (0.016–10 μM) as a single compound as well as in combination with the anti-TNF- α blocking antibody adalimumab ($n = 10$); recombinant CD95L ($n = 10$); the TLR8 agonist, motolimod ($n = 12$); and the Bruton tyrosine kinase/IL-2-inducible T-cell kinase inhibitor ibrutinib ($n = 12$). The addition of adalimumab and ibrutinib reduced birinapant-induced cell death in T-PLL and T-LGL, whereas TLR8 stimulation promoted T-PLL and T-LGL cell killing (CI = 1.75, 1.46, 0.9; adjusted P value = .006, .011, .085; **Figure 5K–M**; supplemental Figure 8D–F). Furthermore, CD95L binding sensitized individual patient samples to birinapant killing (CI = 0.93; adjusted P value = .106; supplemental Figure 8G). This was correlated with the CD95 cell surface expression levels of the malignant cells, as assessed by spectral flow cytometry ($R^2 = -0.84$; adjusted P value = .009; **Figures 5N** and **6A**). Combined, these findings suggest that birinapant-induced cell death in T-PLL and T-LGL requires the binding of TNF- α and the activity of

IL-2-inducible T-cell kinase, whereas TLR, and possibly CD95 pathway signaling, sensitize malignant T-cells.

IAP inhibitors decrease T-PLL proliferation and differentially affect healthy cell subsets

Next, we sought to study the effect of IAP inhibitors on proliferation and cytokine expression in different cellular subsets including nonmalignant cells. To this end, we treated 10 T-PLL, 1 T-LGL and 4 healthy age-matched PBMC samples with either a sublethal concentration of birinapant (0.2 μM) or DMSO for 40 hours, followed by 4 hours stimulation *ex vivo*. We then performed spectral flow cytometry using a 30-marker panel (**Figure 6A–E**; supplemental Figure 9A). In addition to resolution of the T-cell compartment, and the major B-cell and natural killer (NK) cell types (supplemental Figure 9B–C), this panel included 3 distinct cell death markers, Apotransfer Green (early and late cell death), LIVE/DEAD staining (late cell death), and cleaved caspase-3 (apoptotic) to explore the mode of birinapant-induced cell death. Birinapant treatment significantly reduced the frequency of proliferating lymphoma cells but not that of nonmalignant B, T, and NK cells (adjusted P value = .076, .918, .12, .417; **Figure 6F**; supplemental Figure 9D). The effect of birinapant on cytokine expression was cell type dependent (linear mixed model, FDR < 10%). Birinapant treatment significantly increased the expression of TNF- α and granulocyte-macrophage colony-stimulating factor in NK cells and showed a trend for increased IL-2 expression in T cells (adjusted P value = .092, .073, .227; **Figure 6G**; supplemental Figures 9E–J and 10A–B). Next, we sought to explore the mode of birinapant-induced cell death. To this end, we cultured 10 T-PLL, 1 T-LGL, and 4 healthy PBMC samples with either selinexor, birinapant (1 μM) with and without Q-VD-OPh, or DMSO, followed by spectral flow cytometry using the same 30-marker panel (**Figure 6H–K**; supplemental Figure 10C). Both selinexor and birinapant significantly reduced the fraction of live T-PLL and T-LGL cells compared with DMSO (2-sided paired *t* test, FDR < 10%; $\Delta = -0.096$, -0.234 ; adjusted P value = .009, .023; supplemental Figure 10D). Although selinexor led to a significant enrichment of apoptotic cells, birinapant-induced cell death was primarily nonapoptotic (apoptotic: adjusted P value = .04, .801; nonapoptotic: adjusted P value = .023, .003; **Figure 6L–M**). Notably, the addition of Q-VD-OPh greatly

Figure 5. IAP inhibitor-induced cell death mode. (A) Schematic of the different cell death complexes induced by IAP inhibition. Cell death execution steps blocked by Q-VD-OPh, necrostatin-1, NSA, and GSK-872 are indicated. (B) Heat map showing the scaled expression of key apoptotic and necroptotic proteins measured by western blot in cell lysates of patient-derived T-PLL ($n = 8$) samples with varying sensitivity to IAP inhibitors. The annotation bar shows the viability (averaged over all concentrations) of each patient sample after birinapant treatment. (C) Heat map showing the correlation between protein expression (measured by western blot) of key apoptotic and necroptotic proteins and IAP inhibitor response. The Pearson correlation coefficient (R^2) was computed from the viabilities of the 7 T-PLL samples with matching drug response (an eighth patient sample had protein expression, but no drug response), averaged over all concentrations. The rows and columns were arranged based on the hierarchical clustering. Dose response curves of patient-derived T-PLL ($n = 11$) and T-LGL ($n = 1$) samples showing the mean observed combination (AB) and expected combination effect according to the independent effect model (A \times B, supplemental Methods) for birinapant in combination with the RIPK1 inhibitor necrostatin-1 (12.5 μM) (D), the MLKL oligomerization inhibitor NSA (2 μM) (E), the RIPK3 inhibitor GSK-872 (4 μM) (F), and the pan-caspase inhibitor Q-VD-OPh (12.5 μM) (G). Error bars indicate the standard error of the mean. (H) Scatter plot showing the relationship between measured combination effect AB (y-axis) and expected combination effect (A \times B) based on the independent effect model (x-axis) for patient-derived T-PLL ($n = 11$) and T-LGL ($n = 1$) samples for necrostatin-1, NSA, GSK-872, and Q-VD-OPh. (I) Heat map showing the averaged combination effect of Q-VD-OPh (12.5 μM) and necrostatin-1 (12.5 μM) with birinapant in patient-derived T-PLL ($n = 12$), MCL ($n = 15$), CLL ($n = 10$), and other T-cell lymphoma ($n = 10$) samples. Colors show synergy (blue) and antagonism (red), indicated by adjusted P values (2-sided paired *t* test) for each concentration of birinapant. (J) Corresponding heat map showing the combination effect of NSA (2 μM) with birinapant in T-PLL ($n = 12$), MCL ($n = 13$), CLL ($n = 20$), and other T-cell lymphoma ($n = 10$) samples. Dose response curves of T-PLL ($n_{T\text{-PLL}} = 9$) and T-LGL ($n_{T\text{-LGL}} = 1$) samples showing the mean observed (AB) and expected combination effect according to the independent effect model (A \times B) for birinapant in combination with the anti-TNF- α antibody adalimumab (5 $\mu\text{g/mL}$; $n_{T\text{-PLL}} = 9$, $n_{T\text{-LGL}} = 1$) (K), the Bruton tyrosine kinase/IL-2-inducible T-cell kinase inhibitor ibrutinib (2 μM ; $n_{T\text{-PLL}} = 11$, $n_{T\text{-LGL}} = 1$) (L), and the TLR8 agonist motolimod (0.4 μM ; $n_{T\text{-PLL}} = 11$, $n_{T\text{-LGL}} = 1$) (M). (N) Scatterplot showing the pairwise correlation of the CD95 surface protein expression levels (median over all malignant cells per patient) measured by spectral flow and the CI of recombinant human CD95L (5 $\mu\text{g/mL}$) and birinapant (averaged over all concentrations) in T-PLL ($n = 10$) and T-LGL ($n = 1$) samples. A trendline is indicated; 95% confidence intervals are shown as shaded gray areas. Avg. Viab., average viability; Bax, Bcl-2-associated X protein; Bid, BH3 interacting-domain death agonist; Bik, Bcl-2-interacting killer; CI, combination index; FADD, Fas associated via death domain; FLIPS, FLICE-like inhibitory protein short isoform; FLIPL, FLICE-like inhibitory protein long isoform; Expr., expression; MLKL, mixed lineage kinase domain-like pseudokinase; PARP, poly(ADP-ribose)-polymerase; RIPK1/3, receptor interacting serine/threonine kinase 1/3; TRADD, tumor necrosis factor receptor type 1 associated via death domain.

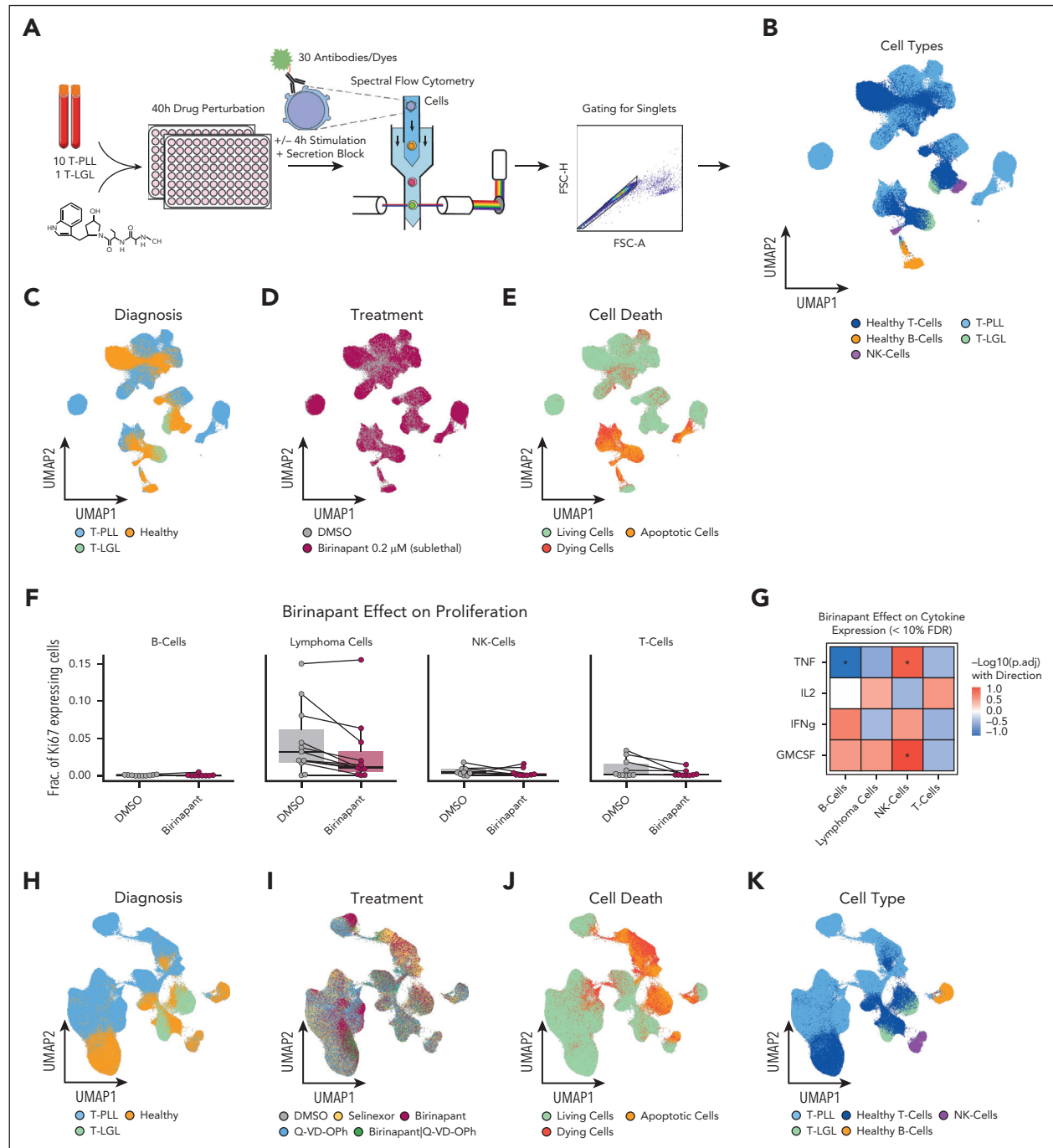


Figure 6. Immune landscape of T-PLL, T-LGL, and healthy donor PBMCs upon IAP inhibition measured by spectral flow cytometry. (A) Schematic overview of the spectral flow cytometry experiments and gating strategy. In the stimulated experiment T-PLL ($n = 10$), T-LGL ($n = 1$), and healthy age-matched PBMC ($n = 4$) samples were treated with either birinapant ($0.2 \mu\text{M}$) or DMSO for 40 hours ex vivo, followed by 4 hours incubation with cytokine secretion block and stimulation with phorbol 12-myristate 13-acetate (PMA; $0.1 \mu\text{g}/\text{mL}$) and ionomycin ($1 \mu\text{g}/\text{mL}$). In the unstimulated experiment, the same patient samples were treated with either selinexor ($1 \mu\text{M}$), birinapant ($1 \mu\text{M}$) with and without Q-VD-OPh ($12.5 \mu\text{M}$), or DMSO for 40 hours ex vivo, followed by 4 hours incubation with cytokine secretion block. In both experiments, cells were subsequently stained with 30 fluorescently labeled antibodies and dyes and processed for spectral flow cytometry. After acquisition, events were gated for single cells based on FSC-A and FSC-H. (B) UMAP representation of the spectral flow cytometry data derived from patient and healthy donor samples treated with birinapant ($0.2 \mu\text{M}$) or DMSO followed by subsequent stimulation. Major cell types are indicated by color. Corresponding UMAP representations colored by diagnosis (C), treatment (D), and cell death (E). (F) Box plot showing the fraction of proliferating cells per cell type for birinapant ($0.2 \mu\text{M}$) or DMSO treatment followed by subsequent stimulation. (G) Heat map showing the effect of treatment with birinapant ($0.2 \mu\text{M}$) on median cytokine expression per cell type compared with DMSO. Colors show increased (red) and decreased (blue) median expression, indicated by adjusted P values (linear mixed model; FDR $< 10\%$). Significant effects are indicated with a star. (H) UMAP representation of the spectral flow cytometry data derived from patient and healthy donor samples treated with selinexor ($1 \mu\text{M}$), birinapant ($1 \mu\text{M}$) with and without Q-VD-OPh ($12.5 \mu\text{M}$), or DMSO. Diagnosis is indicated by color. Corresponding UMAP representation colored by treatment (I), cell death (J), and major cell types (K). (L) Box plot showing the fraction of apoptotic (cleaved caspase 3 positive) dying cells per cell type for patient and healthy donor samples treated with selinexor ($1 \mu\text{M}$) or birinapant ($1 \mu\text{M}$) with and without Q-VD-OPh ($12.5 \mu\text{M}$) relative to the DMSO negative controls. Each dot represents a patient, observations outside the plotting range are censored and shown as triangles. (M) Corresponding plot showing the fraction of nonapoptotic dying cells (cleaved caspase 3 negative). (N) Bar plot showing the mean frequency of cell subtypes among all living cells in selinexor-treated ($1 \mu\text{M}$) healthy donor samples relative to DMSO. (O) Corresponding bar plot for birinapant ($1 \mu\text{M}$). FSC-A, forward scatter area; FSC-H, forward scatter height; h, hour; p.adj., adjusted P value; Rel., relative.

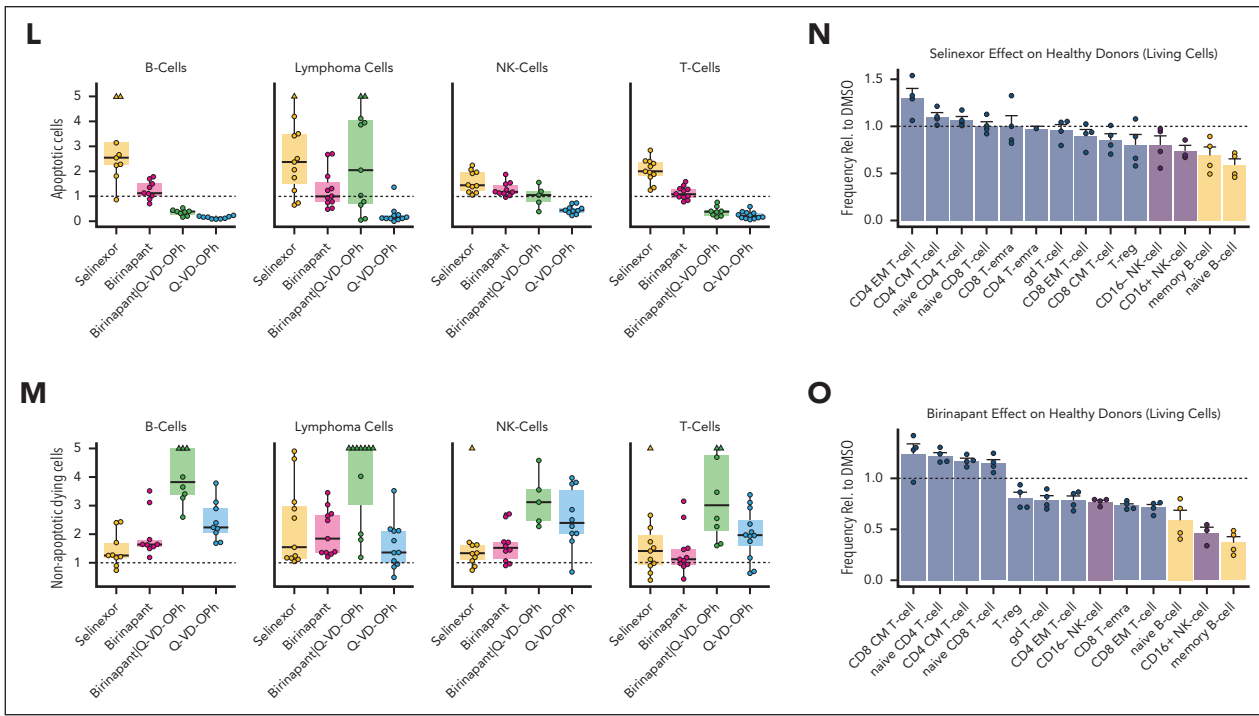


Figure 6 (continued)

increased birinapant killing of lymphoma cells but not of nonmalignant B, T, and NK cells, a finding consistent with necroptosis through caspase-8 inhibition ($\Delta = 0.39, 1.38, 0.88, 0.95$; adjusted P value = .065, .834, .898, .898; supplemental Figure 10D).^{31,42,43} Among the nonmalignant cells, selinexor treatment significantly decreased the viability of B, T, and NK cells ($\Delta = -0.35, -0.22, -0.14$; adjusted P value = .006, .006, .013; supplemental Figure 10D). This effect was pronounced for B and NK cells and resulted in a relative depletion of B-cell and NK cell subtypes among the living cells of the healthy PBMC donors (Figure 6N). Birinapant also decreased the fraction of live B and NK cells but did not affect the overall fraction of live nonmalignant T cells ($\Delta = -0.14, -0.08, -0.08$; adjusted P value = .023, .002, .124; supplemental Figure 10D). We did, however, observe a trend toward the enrichment of naive and central memory CD4 and CD8 T cells among the living cells of healthy donor PBMCs, suggesting that birinapant treatment might differentially affect T-cell subsets (Figure 6O). In summary, spectral flow cytometry demonstrated that birinapant reduces T-cell lymphoma proliferation at sublethal concentrations and induces non-apoptotic death, whereas showing only a limited effect on nonmalignant immune cells.

Discussion

Here, we report on drug vulnerabilities of T-PLL to exportin 1 (selinexor), autophagy (bafilomycin A1), and IAP (birinapant) inhibition, that were shared by other T-cell malignancies. To characterize the biological processes behind these vulnerabilities, we used spectral flow cytometry and bulk and scRNA-seq to study T-PLL drug response. We found the response of selinexor to be significantly correlated with that of nutlin-3a in our drug screening data and could subsequently demonstrate the upregulation of TP53 and its target genes after selinexor treatment.

Bafilomycin A1, a strong inhibitor of autophagy, demonstrated considerable transcriptional overlap with the TLR8 agonist motolimod. This suggests that in addition to its effects on cell metabolism, bafilomycin A1 promotes TLR pathway activation in T-PLL, as has been proposed for human monocytes.²⁸ We explored the sensitivity of T-PLL to the IAP inhibitor birinapant, which is known to induce cell death through either apoptosis or necroptosis.^{31,37} The dependence on RIPK1 and RIPK3 kinase activity, as well as MLKL activation in our drug combination experiments, combined with the lack of caspase-3 cleavage in our spectral flow cytometry data indicate that birinapant-induced cell death in T-PLL is primarily necroptotic. Indeed, the addition of the pan-caspase inhibitor Q-VD-OPh further sensitized lymphoma but not nonmalignant cell types to birinapant killing, likely by promoting necroptosis through caspase-8 inhibition.^{31,42,43} The opposite effect was observed in B-cell lymphomas, in which birinapant-induced cell death was primarily RIPK1-independent and apoptotic. This was surprising given that T-PLL, T-LGL, MCL, and HCL cells showed a similar transcriptional activation of the TNF- α /NF- κ B pathway after birinapant treatment in our scRNA-seq data and highlights the intricacy of the multiprotein signaling complexes that form after IAP depletion. We observed a limited effect of birinapant on nonmalignant T-cell transcriptomes and viability. These findings are in line with reports that show a limited impact of birinapant on healthy T-cell viability and even enhanced tumor cell killing of chimeric antigen receptor T cells after birinapant treatment.^{44,45} Combined, these findings suggest that IAP inhibitors are not generally toxic for healthy T cells.

Previous studies have described T-PLL sensitivity to BH3 mimetics, p53 activators, as well as HDAC and JAK-STAT inhibitors.³⁻⁷ Early clinical data, however, suggest that these compounds are insufficient to provide long-term control of the disease.^{6,8} Recently, Jan et al have reported synergistic drug combinations for the treatment of T-PLL.⁹ By screening 8 drug classes with previously

reported single-agent activity, the authors demonstrated encouraging results for combinations involving the p53 activator idasanutlin, the HDAC inhibitor romidepsin, and the ribonucleotide reductase inhibitor cladribine, based on the superior ability of these combinations to activate the p53 pathway.⁹ We now report on T-PLL sensitivity to >2800 compounds and identify hitherto unexplored drug vulnerabilities of T-PLL. Notably, each of the compounds (birinapant, selinexor, and bafilomycin A1), demonstrated distinct pathway dependencies, making them optimal candidates to explore drug combinations to circumvent intrinsic and acquired resistances (ie, TP53 escape mutations). Furthermore, birinapant and selinexor have demonstrated manageable toxicity in phase 2 clinical trials, which could facilitate their further clinical development in T-PLL and other T-cell malignancies.^{35,46}

Acknowledgments

The authors thank Jan Dürig and Marco Herling for the contribution of samples; Berend Snijder, Julien Mena, Steffen Böttcher, and Roman Schimmer for input on the design and the printing of combinatorial drug plates; and André Samson for his insights on the necroptotic signaling cascade.

This work was supported by the KFSP Precision Hematology and Oncology, the Helmut Horten Foundation, and The LOOP Zurich (INTeRCePT).

M.F.P. is an MD thesis candidate at the University of Zurich, and this work is submitted in partial fulfillment of the requirement for the MD thesis.

Authorship

Contribution: J. Lewis, W.H., and T.Z. devised the research strategy; A.M. cosupervised the research; M.F.P., K.P., S.S., L.B.T., T. Walther, S. Kummer, T. Wertheimer, M.L., T.H.L.D., K.H., J.M., S. Kisele, J. Kim, and J. Kivioja performed the experiments; M.F.P. and J. Lu performed data analyses; J. Lu, M.F.P., and K.B. developed the tools; K.B., X.F., W.H., W.W.-L.W., and T.Z. helped to interpret results; T.Z., J. Lewis, W.H., S.D., A.M., B. Becher, and B. Bornhauser provided resources; M.F.P., J. Lu, X.F., and T.Z. wrote the manuscript; and all authors reviewed the manuscript before submission.

REFERENCES

1. Staber PB, Herling M, Bellido M, et al. Consensus criteria for diagnosis, staging, and treatment response assessment of T-cell prolymphocytic leukemia. *Blood*. 2019; 134(14):1132-1143.
2. Cross MJ, Else M, Morilla R, et al. No improvement in survival for T-PLL patients over the last two decades [abstract]. *Blood*. 2019;134(suppl 1):1552.
3. Andersson EI, Pützer S, Yadav B, et al. Discovery of novel drug sensitivities in T-PLL by high-throughput ex vivo drug testing and mutation profiling. *Leukemia*. 2018;32(3): 774-787.
4. Herbaux C, Kornauth C, Poulain S, et al. BH3 profiling identifies ruxolitinib as a promising partner for venetoclax to treat T-cell prolymphocytic leukemia. *Blood*. 2021; 137(25):3495-3506.
5. Dietrich S, Oleś M, Lu J, et al. Drug-perturbation-based stratification of blood cancer. *J Clin Invest*. 2018;128(1):427-445.
6. Boidol B, Kornauth C, van der Kouwe E, et al. First-in-human response of BCL-2 inhibitor venetoclax in T-cell prolymphocytic leukemia. *Blood*. 2017;130(23):2499-2503.
7. Schrader A, Crispatz G, Oberbeck S, et al. Actionable perturbations of damage responses by TCL1/ATM and epigenetic lesions form the basis of T-PLL. *Nat Commun*. 2018;9(1):697.
8. Hampel PJ, Parikh SA, Call TG, et al. Venetoclax treatment of patients with relapsed T-cell prolymphocytic leukemia. *Blood Cancer J*. 2021;11(3):47.
9. von Jan J, Timonen S, Braun T, et al. Optimizing drug combinations for T-PLL: restoring DNA damage and P53-mediated apoptotic responses. *Blood*. 2024;144(15): 1595-1610.
10. Jethwa A, Hüllein J, Stolz T, et al. Targeted resequencing for analysis of clonal composition of recurrent gene mutations in chronic lymphocytic leukaemia. *Br J Haematol*. 2013;163(4):496-500.
11. Meier-Abt F, Lu J, Cannizzaro E, et al. The protein landscape of chronic lymphocytic leukemia. *Blood*. 2021;138(24): 2514-2525.
12. Lukas M, Velten B, Sellner L, et al. Survey of ex vivo drug combination effects in chronic lymphocytic leukemia reveals synergistic drug effects and genetic dependencies. *Leukemia*. 2020;34(11):2934-2950.
13. Wei J, Stebbins JL, Kitada S, et al. BI-97C1, an optically pure apogossypol derivative as pan-active inhibitor of antiapoptotic B-cell lymphoma/leukemia-2 (Bcl-2) family proteins. *J Med Chem*. 2010;53(10):4166-4176.
14. Souers AJ, Leverson JD, Boghaert ER, et al. ABT-199, a potent and selective BCL-2 inhibitor, achieves antitumor activity while sparing platelets. *Nat Med*. 2013;19(2): 202-208.
15. Tse C, Shoemaker AR, Adickes J, et al. ABT-263: a potent and orally bioavailable Bcl-2 family inhibitor. *Cancer Res*. 2008;68(9): 3421-3428.

Conflict-of-interest disclosure: The authors declare no competing financial interests.

ORCID profiles: M.F.P., 0000-0003-0393-5840; K.P., 0000-0001-8375-5908; T. Wertheimer, 0000-0002-8480-7391; T.H.L.D., 0000-0001-8058-4410; K.H., 0000-0001-8952-6487; J.M., 0000-0002-6382-9145; J. Kivioja, 0000-0002-4046-0963; K.B., 0000-0003-3622-1115; S. Kisele, 0000-0003-0369-7854; J. Kim, 0000-0002-8996-2569; B. Bornhauser, 0000-0003-2890-3191; W.W.-L.W., 0000-0003-3155-1211; B. Becher, 0000-0002-1541-7867; A.M., 0000-0001-8715-8449; J. Lewis, 0000-0002-9926-1328; X.F., 0000-0002-4534-8225; J. Lu, 0000-0002-9211-0746; W.H., 0000-0002-0474-2218; T.Z., 0000-0001-7890-9845.

Correspondence: Thorsten Zenz, Department of Medical Oncology and Hematology, University Hospital Zurich, Rämistr 100, CH-8091 Zürich, Switzerland; email: thorsten.zenz@usz.ch; Wolfgang Huber, European Molecular Biology Laboratory, Meyerhofstr 1, 69117 Heidelberg, Germany; email: wolfgang.huber@embl.org; and Junyan Lu, Medical Faculty Heidelberg, Heidelberg University, Im Neuenheimer Feld 130.3, 69120 Heidelberg, Germany; email: junyan.lu@uni-heidelberg.de.

Footnotes

Submitted 10 October 2024; accepted 1 January 2025; prepublished online on Blood First Edition 27 January 2025. <https://doi.org/10.1182/blood.2024027171>.

Bulk and scRNA-seq data have been deposited with Zenodo. The data can be accessed at <https://zenodo.org/records/14603672>.

Drug screening data and spectral flow cytometry data are available upon reasonable request from the corresponding authors, Thorsten Zenz (thorsten.zenz@usz.ch), Wolfgang Huber (wolfgang.huber@embl.org), and Junyan Lu (junyan.lu@uni-heidelberg.de). All codes used to generate figures can be found at <https://github.com/Moors-Code/TPLLdrugscreen>.

The online version of this article contains a data supplement.

There is a *Blood Commentary* on this article in this issue.

The publication costs of this article were defrayed in part by page charge payment. Therefore, and solely to indicate this fact, this article is hereby marked "advertisement" in accordance with 18 USC section 1734.

16. Nguyen M, Marcellus RC, Roulston A, et al. Small molecule obatoclax (GX15-070) antagonizes MCL-1 and overcomes MCL-1-mediated resistance to apoptosis. *Proc Natl Acad Sci U S A*. 2007;104(49):19512-19517.
17. Mohammad RM, Goustin AS, Aboukameel A, et al. Preclinical studies of TW-37, a new nonpeptidic small-molecule inhibitor of Bcl-2, in diffuse large cell lymphoma xenograft model reveal drug action on both Bcl-2 and Mcl-1. *Clin Cancer Res*. 2007;13(7):2226-2235.
18. Horwitz SM, Koch R, Porcu P, et al. Activity of the PI3K- δ,γ inhibitor duvelisib in a phase 1 trial and preclinical models of T-cell lymphoma. *Blood*. 2018;131(8):888-898.
19. Moskowitz AJ, Ghione P, Jacobsen E, et al. A phase 2 biomarker-driven study of ruxolitinib demonstrates effectiveness of JAK/STAT targeting in T-cell lymphomas. *Blood*. 2021;138(26):2828-2837.
20. Dearden C. How I treat prolymphocytic leukemia. *Blood*. 2012;120(3):538-551.
21. Kucab JE, Hollstein M, Arlt VM, Phillips DH. Nutlin-3a selects for cells harbouring TP53 mutations. *Int J Cancer*. 2017;140(4):877-887.
22. Mitsuchi Y, Benetatos CA, Deng Y, et al. Bivalent IAP antagonists, but not monovalent IAP antagonists, inhibit TNF-mediated NF- κ B signaling by degrading TRAF2-associated cIAP1 in cancer cells. *Cell Death Discov*. 2017;3(1):16046.
23. Fischer M. Census and evaluation of p53 target genes. *Oncogene*. 2017;36(28):3943-3956.
24. Kanehisa M, Goto S. KEGG: Kyoto encyclopedia of genes and genomes. *Nucleic Acids Res*. 2000;28(1):27-30.
25. Kanehisa M, Furumichi M, Sato Y, Kawashima M, Ishiguro-Watanabe M. KEGG for taxonomy-based analysis of pathways and genomes. *Nucleic Acids Res*. 2023;51(D1):D587-D592.
26. Gilmore, T. NF- κ B transcription factors. Accessed 30 April 2023. <https://www.bu.edu/nf-kb/gene-resources/target-genes/>
27. Kanehisa M. Toward understanding the origin and evolution of cellular organisms. *Protein Sci*. 2019;28(11):1947-1951.
28. Yu S, Green J, Wellens R, Lopez-Castejon G, Brough D. Bafilomycin A1 enhances NLRP3 inflammasome activation in human monocytes independent of lysosomal acidification. *FEBS J*. 2021;288(10):3186-3196.
29. Bertrand MJM, Milutinovic S, Dickson KM, et al. cIAP1 and cIAP2 facilitate cancer cell survival by functioning as E3 ligases that promote RIP1 ubiquitination. *Mol Cell*. 2008;30(6):689-700.
30. Geserick P, Hupe M, Moulin M, et al. Cellular IAPs inhibit a cryptic CD95-induced cell death by limiting RIP1 kinase recruitment. *J Cell Biol*. 2009;187(7):1037-1054.
31. Feoktistova M, Geserick P, Kellert B, et al. cIAPs block ripoptosome formation, a RIP1/caspase-8 containing intracellular cell death complex differentially regulated by cFLIP isoforms. *Mol Cell*. 2011;43(3):449-463.
32. Tenev T, Bianchi K, Darding M, et al. The ripoptosome, a signaling platform that assembles in response to genotoxic stress and loss of IAPs. *Mol Cell*. 2011;43(3):432-448.
33. Lawlor KE, Feltham R, Yabal M, et al. XIAP loss triggers RIPK3- and caspase-8-driven IL-1 β activation and cell death as a consequence of TLR-MyD88-induced cIAP1-TRAF2 degradation. *Cell Rep*. 2017;20(3):668-682.
34. Condon SM, Mitsuchi Y, Deng Y, et al. Birinapant, a smac-mimetic with improved tolerability for the treatment of solid tumors and hematological malignancies. *J Med Chem*. 2014;57(9):3666-3677.
35. Noonan AM, Bunch KP, Chen J-Q, et al. Pharmacodynamic markers and clinical results from the phase 2 study of the SMAC mimetic birinapant in women with relapsed platinum-resistant or -refractory epithelial ovarian cancer. *Cancer*. 2016;122(4):588-597.
36. Dietrich S, Glimm H, Andrusis M, von Kalle C, Ho AD, Zenz T. BRAF inhibition in refractory hairy-cell leukemia. *N Engl J Med*. 2012;366(21):2038-2040.
37. McComb S, Aguadé-Gorgorió J, Harder L, et al. Activation of concurrent apoptosis and necroptosis by SMAC mimetics for the treatment of refractory and relapsed ALL. *Sci Transl Med*. 2016;8(339):339ra70.
38. Murphy JM, Czabotar PE, Hildebrand JM, et al. The pseudokinase MLKL mediates necroptosis via a molecular switch mechanism. *Immunity*. 2013;39(3):443-453.
39. Wang L, Du F, Wang X. TNF- α induces two distinct caspase-8 activation pathways. *Cell*. 2008;133(4):693-703.
40. Varfolomeev E, Blankenship JW, Wayson SM, et al. IAP antagonists induce autoubiquitination of c-IAPs, NF- κ B activation, and TNF α -dependent apoptosis. *Cell*. 2007;131(4):669-681.
41. Vince JE, Wong WW-L, Khan N, et al. IAP antagonists target cIAP1 to induce TNF α -dependent apoptosis. *Cell*. 2007;131(4):682-693.
42. Oberst A, Dillon CP, Weinlich R, et al. Catalytic activity of the caspase-8-FLIPL complex inhibits RIPK3-dependent necrosis. *Nature*. 2011;471(7338):363-367.
43. Laukens B, Jennewein C, Schenk B, et al. Smac mimetic bypasses apoptosis resistance in FADD- or caspase-8-deficient cells by priming for tumor necrosis factor α -induced necroptosis. *Neoplasia*. 2011;13(10):971-979.
44. Burton A, Ligman B, Kearney C, Murray SE. Clinically relevant SMAC mimetics do not enhance human T cell proliferation or cytokine production. *bioRxiv*. Preprint posted online 11 November 2021. <https://doi.org/10.1101/2021.11.09.466489>
45. Dufva O, Koski J, Maliniemi P, et al. Integrated drug profiling and CRISPR screening identify essential pathways for CAR T-cell cytotoxicity. *Blood*. 2020;135(9):597-609.
46. Chari A, Vogl DT, Gavriatopoulou M, et al. Oral selinexor-dexamethasone for triple-class refractory multiple myeloma. *N Engl J Med*. 2019;381(8):727-738.

© 2025 American Society of Hematology. Published by Elsevier Inc. All rights are reserved, including those for text and data mining, AI training, and similar technologies.